Theoretical Investigation of Electronic Structures and Properties of C_{60}—Gold Nanocontacts

Manoj K. Shukla,[†] Madan Dubey,[‡] and Jerzy Leszczynski[†,*]

[†]Computational Centre for Molecular Structure and Interactions, Department of Chemistry, Jackson State University, Jackson, Mississippi 39217, and [‡]U.S. Army Research Laboratory, Sensors and Electron Devices Directorate, AMSRD-ARL-SE-RL, Adelphi, Maryland 20783

ABSTRACT A theoretical study was performed to understand the structures and properties of C_{60}—gold nanocontacts. In this investigation, C_{60} was sandwiched between gold clusters. In the studied clusters, the number of Au atoms varied from 2 to 8 on each side of C_{60}. Molecular geometries of the investigated complexes were optimized at the density functional theory level, employing the B3LYP functional. The 6-31G(d) basis set was used for carbon atoms, while the LANL2DZ effective core potential was used for gold atoms. Geometries of all complexes were optimized under C_{2h} symmetry except for the C_{60}—10Au complex, for which C_2 symmetry was assumed. Two different configurations, namely $\eta^{2(5)}$ and $\eta^{2(6)}$, for the binding of Au clusters with C_{60} were considered. It was revealed that complexes corresponding to the latter configuration are more stable than those having the former one. Ground-state geometries of the complexes involving odd numbers of gold atoms on each side of C_{60} were found to be represented by the triplet configuration. The HOMO–LUMO energy gaps of C_{60}—gold complexes were found to be lower than that of isolated C_{60}. The charge transport properties in the studied system are discussed in terms of molecular orbitals and the Fermi level.

KEYWORDS: C_{60} · gold cluster · nanocontact · charge transfer · nanomaterials · Fermi level

The discovery of fullerene (C_{60}) in 1985 by Kroto *et al.*,[1] and subsequent enormous progress in and development of different carbon-based structures, started a renaissance of tailored designing of nanomaterials.[2–5] Nanomaterials are now increasingly being used in different aspects of human life. Among their recent applications are microelectronics, semiconductors, space applications, drug delivery systems, sporting goods, cosmetics, sunscreens, stain-resistant clothing, and many more. Interestingly, an issue of *Chemical & Engineering News* revealed that some exotic cosmetics with embedded fullerene nanoparticles are in the market.[6] Detailed information about the synthesis, structures, properties, and interactions of different nanoclusters and nanodevices can be found in recent review articles.[4,5,7–10] Important characteristics of nanoparticles include the dependence of their physical properties on particle size, internuclear distance, and shape of these nanomaterials. Such unique aspects significantly differentiate them from both the bulk metals and the molecular compounds.[11] For example, the absorption maxima of gold nanoparticles red-shift with the particle size.[9] Recently, using density functional theory (DFT) calculations, we have shown that, by changing the shape and size of carbon nanoclusters, it is possible to design nanomaterials with different conducting properties.[12]

During the past few years, significant effort has been made to understand electron transport in nanostructures including nanocrystals, nanotubes, and molecular devices.[13–15] Park *et al.*[16] reported the fabrication of C_{60}-based single-molecule transistors in which fullerene was connected to gold electrodes. The transport measurement indicated the coupling of motion of the center of mass of C_{60} and single-electron hopping; the frequency of oscillation of C_{60} between gold electrodes esd about 1.2 THz. Seideman and co-workers[17–19] have extensively studied current-induced oscillation in Au—C_{60}—Au heterojunctions using theoretical methods. In their investigations, a C_{60} molecule was sandwiched between two modeled Au electrodes, where the Au atoms were oriented along the (100) plane and the distance between the electrode surface and the C_{60} side was 2.3 Å. It was revealed that the excitation of vibrational motion of C_{60} between electrodes was due to the deposition of energy to the center-of-mass motion of fullerene consequent to the current passing through the device. The tight binding scheme within DFT has also been extensively and successfully used to study the band structure of different nanoclusters and nanotubes and their interactions with metal clusters.[20–22] The Gaussian embedded

*Address correspondence to jerzy@ccmsi.us.

Received for review July 2, 2007 and accepted January 20, 2008.

Published online February 26, 2008.
10.1021/nn700080p CCC: $40.75

cluster method (GECM) scheme has been developed to investigate electron transport properties of different nanoclusters between different electrodes.[23–26] Nakamura and Yamashita[27] and Sergueev *et al.*[28] have independently studied transport properties in molecular junctions by using nonequilibrium Green's function in combination with DFT.

Since device miniaturization is an important aspect of molecular electronics, a reliable and thorough understanding of the nature of metallic contact with materials is necessary for understanding the transport properties in nanodevices. The electrical transport properties of carbon nanotubes (CNTs) are significantly influenced by the nature of the nanocontacts; contact resistance poses a serious problem in understanding the intrinsic electrical properties of CNTs.[29–31] In Au/C_{60}/p-Si sandwich structures, the *I–V* characteristic was found to be ohmic.[32] Fullerene-based materials have also been considered as prospective materials for photovoltaic cells,[33] but the main challenge is to find a way to increase the efficiency of conduction in these materials to create efficient fullerene-based solar cells. Gold nanoparticles are also of interest due to their possible use as guest hybrid materials for applications in sensors and as catalysts. Recently, it has been reported that hybridization of single-walled carbon nanotubes (SWNTs) with gold nanoparticles increases the electrical conductivity by 2-fold, and such hybridization does not change the transmittance of the hybrid structure compared to that of the neat SWNT film.[34]

The coordination of metals with the C_{60} surface is a complex phenomenon, and such interactions depend significantly on the nature of the metals used in the investigation.[35–38] On the basis of the IR spectra of a Au−C_{60} complex, Lyon and Andrews[36] have suggested the possibility of binding of Au to the pentagonal ring of C_{60}. On the other hand, on the basis of a B3LYP level of calculation with the STO-3G* basis set for carbon and SDD for gold, the same authors have found different types of coordinations,[36] which are in agreement with computed results for silver complexes. Lichtenberger *et al.*[37,38] have studied the bonding of palladium atoms and silver(I) ions with the five bonding sites of C_{60}, namely (i) a single carbon atom (η^1-coordination), (ii) above the center of fused six-membered rings (η^2-coordination), (iii) the center of fused five- and six-membered rings, (iv) above the center of pentagonal rings (η^5-coordination), and (v) the center of hexagonal rings (η^6-coordination). The η^2-coordination was favored among all bonding sites. Seminario and coworkers[39] have studied the electron transport properties of group 10 and group 11 metals with thio and isonitrile alligator clips using the B3PW91/LANL2DZ level and the Green function approach. The performance of group 10 metals at the metal−molecule interface was found to be significantly better than that of the group 11 metals, and particularly the performance of Pd was revealed as the best and that of Au and Ag was found to be significantly inferior.[39]

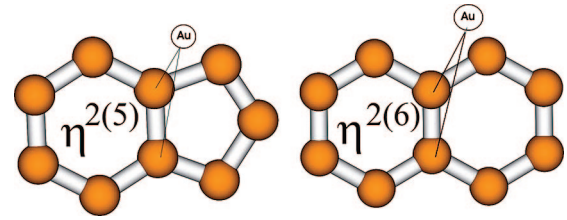

Figure 1. Bonding configurations of Au clusters with C_{60}.

In theoretical modeling of electron transport through C_{60} and CNTs placed between electrodes, the surfaces of the electrodes are generally idealized. It is well-known that the overall performance of electronic devices is influenced by the nature of the contacts and it is crucial to lower the contact resistance to achieve a definite understanding of the intrinsic electrical properties of nanodevices. The actual atomic structures of the electrodes, especially at the point of contact, are not known. It is expected that the actual surface would be rough and the structure at the point of contact would vary from sample to sample, even when fabricated under the same conditions. Thus, it appears that, at the point of contact, only a few atoms from the electrodes would be involved in interactions with the materials. It should be noted that the number of points of contact would also depend upon the size of the atomic clusters on the electrode surface in contact with material, and this is of immense importance for nanodevices. This study is devoted to understanding the structures and properties of nanocontacts involving C_{60} sandwiched between gold clusters of different sizes, modeling the nanocontacts.

RESULTS AND DISCUSSION

Two types of binding configurations were considered, corresponding to the bonding of Au clusters at the top of the center of fused six-membered rings ($\eta^{2(6)}$-coordination) and that of the fused six- and five-membered rings ($\eta^{2(5)}$-coordination) (Figure 1). The B3LYP-optimized geometries of the complexes are shown in Figures 2 and 3. In these complexes, C_{60} was placed between Au clusters (*n*Au−C_{60}−*n*Au). The clusters on each side of fullerene were obtained by the systematic addition of Au atoms on both sides of C_{60}. Therefore, for the C_{60}−*n*Au complex, where *n* represents the total number of Au atoms, there are *n*/2 atoms on each side of C_{60} (*n*/2Au−C_{60}−*n*/2Au). We have considered complexes of up to eight Au atoms on each side of C_{60}. Geometries were optimized under C_{2h} symmetry, except for the C_{60}−10Au complex, for which C_2 symmetry was obtained. The coordination distance, interaction energy, and amount of Mulliken charge transfer in the studied complexes are shown in Table 1. Here, we would like to point out that we have also optimized the geometry of the C_{60}−4Au complex

under η^1-coordination (single carbon atom binding) within the C_{2h} symmetry, but optimization converged to the $\eta^{2(6)}$-coordination geometry.

It is evident from Table 1 that the Au−C coordination distance is smaller for $\eta^{2(6)}$-type complexes than for $\eta^{2(5)}$-type complexes. The coordination distance for the C_{60}−10Au complex is similar for both types of complexes. This similarity is due to the fact that, in this complex, Au clusters are involved in the η^1-coordination (bonded to only one carbon atom), and thus this structure represents a different type of anchoring. For the $\eta^{2(5)}$-type complexes, the Au−C distance is generally about 2.4 Å, except for the C_{60}−16Au complex. In the case of the $\eta^{2(6)}$-type complexes, the Au−C distance for the larger complexes is smaller than the one in the smaller complexes.

The basis set superposition error (BSSE)-corrected values of the interaction energies, obtained by considering the interaction as a three-body term, shown in Table 1, suggest that C_{60} forms stable complexes with gold clusters. Further, the complexes involving $\eta^{2(6)}$-coordination are significantly more stable than those involving $\eta^{2(5)}$-coordination. Thus, our computed results are in agreement with earlier investigations,[37,38] where complexes of palladium atoms and silver(I) ions with C_{60} involving $\eta^{2(6)}$-type bonding were predicted to be more stable than those with the other types of coordination. Further, in general, the interaction energy was found to increase with the size of the Au cluster for the $\eta^{2(6)}$-type bonding, but such a trend was not revealed for the $\eta^{2(5)}$-type coordination. Thus, it appears that $\eta^{2(6)}$-coordination is more important for nanocontacts, and it is more likely that such structures will be present in the real system. For the larger clusters, the predicted interaction energy is in the range of 35–39 kcal/mol. Several investigations have been performed to study the growth of fullerene thin films and monolayers on the gold surface.[40–42] The adsorption energy is estimated to be around 40–60 kcal/mol.[40,41] Thus, our results of computed interaction energy for $\eta^{2(6)}$-type complexes are in agreement with the estimated adsorption energy data. It is also expected that such agreement would be better for clusters involving larger numbers of gold atoms interacting with C_{60}. It should be noted that, with larger clusters, more coordination sites for bonding of gold atoms with C_{60} are expected, and these additional interactions would strongly stabilize the whole complex.

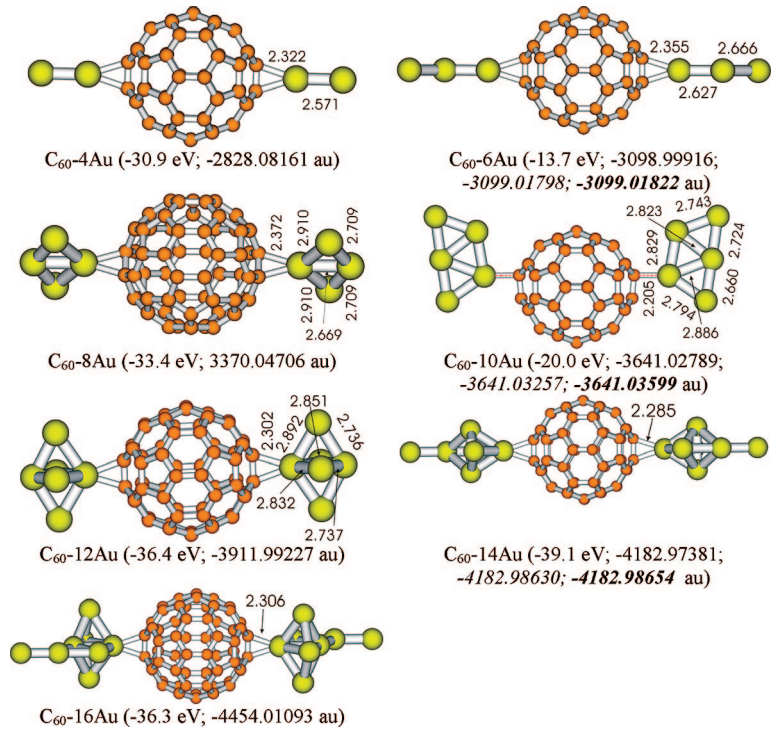

Figure 2. Optimized geometries (singlet state) of C_{60}−gold complexes in $\eta^{2(6)}$-coordination. For each complex, the first value represents the interaction energy (in eV), the second is the optimized singlet ground-state total energy, the third (in italics) is the single-point ground-state triplet energy, and the last one (in bold italics) is the optimized triplet ground-state total energy.

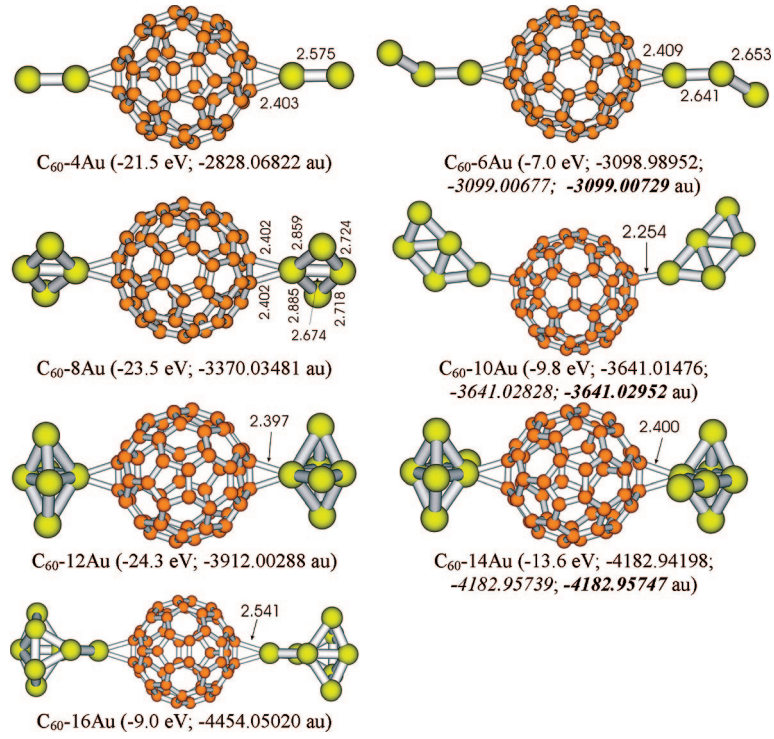

Figure 3. Optimized geometries (singlet state) of C_{60}−gold complexes in $\eta^{2(5)}$-coordination. For each complex, the first value represents the interaction energy (in eV), the second is the optimized singlet ground-state total energy, the third (in italics) is the single-point ground-state triplet energy, and the last one (in bold italics) is the optimized triplet ground-state total energy.

TABLE 1. Computed Au−C distances (Å), Mulliken Charges (in au) on Each Au Cluster, BSSE Values (Hatrees), BSSE-Corrected Interaction Energies (ΔE_{int}, kcal/mol), HOMO–LUMO Energy Gap (H-L, eV), and Fermi Level Energy (E_{FL}, eV) of $\eta^{2(5)}$ and $\eta^{2(6)}$ Types of C_{60}−Gold Complexes[a]

	$\eta^{2(5)}$-coordination					$\eta^{2(6)}$-coordination					
complex	Au−C	charge	ΔE_{int}	BSSE	H-L[b]	Au−C	charge	ΔE_{int}	H-L[b]	BSSE	E_{FL}[c]
C_{60}−4Au	2.403	−0.155	−21.5	0.0118	2.2	2.322	−0.139	−30.9	2.37	0.0146	−5.06
C_{60}−6Au	2.409	−0.128	−7.0	0.0130	0.23 (1.53)	2.355	−0.200	−13.7	0.23 (1.60)	0.0130	−5.03
C_{60}−8Au	2.402	−0.194	−23.5	0.0137	1.60	2.372	−0.197	−33.4	1.80	0.0137	−4.91
C_{60}−10Au	2.205	−0.095	−9.8	0.0125	0.28 (1.22)	2.205	−0.048	−20.0	0.50 (1.25)	0.0147	−4.75
C_{60}−12Au	2.397	−0.205	−24.3	0.0063	1.50	2.302	−0.143	−36.4	2.12	0.0180	−4.86
C_{60}−14Au	2.400	−0.228	−13.6	0.0180	0.21 (1.41)	2.285	−0.088	−39.1	0.31 (1.35)	0.0168	−4.96
C_{60}−16Au	2.541	−0.174	−9.0	0.0110	1.89	2.306	−0.181	−36.3	2.01	0.0047	−5.07

[a]Interaction energy calculation as a three-body term; Mulliken charges are on each gold cluster of the complex. [b]Values in parentheses corresponds to those obtained from the single-point energy calculation of the triplet state using the reference singlet ground-state optimized geometry. [c]Computed value for C_{60} is −4.61 eV.

The computed Mulliken charges on each side of Au cluster, shown in Table 1, suggests that generally a significant amount of charge transfer takes place from C_{60} to gold atoms. Due to symmetry, the amount of charge transferred on each side of the gold clusters should be the same. Evidently, C_{60} acquires equal amounts of positive charge; thus, the interactions of C_{60} between gold clusters would be dominated by electrostatic interactions. However, a clear trend connecting the amount of charge transferred from C_{60} to the gold cluster with the number of gold atoms cannot be established. In another investigation, in which Kumar *et al.*[43] studied the interaction of gold clusters (four and eight atoms) with guanine-cytosine (GC) and adenine-thymine (AT) DNA base pairs at the DFT level, employing the B3LYP functional, a significant amount of electronic charge transfer from the base pairs to the corresponding gold clusters was revealed.

The distribution of Mulliken charges in the form of a color plot (varying color of atoms in the complex, red being the most negative and green being the most positive charged atoms) is shown in Figure 4. The amount of the Mulliken charge (in atomic units) at important atomic sites is also shown in the figure. It is evident that the most negative charges are generally localized on gold clusters, except for the C_{60}−12Au complex, where C−C atoms of C_{60} bonded with gold atoms have the largest negative charge. Further, in general, the gold atoms involved in direct bonding with C_{60} have significant positive charge. In fact, for most of the complexes, they possess the maximum amount of positive charge. However, the complementary carbon atoms of C_{60} involved in direct interactions with gold clusters generally have smaller negative charge. Further, interactions of gold clusters have mainly a localized effect on C_{60}: most atoms of C_{60} have electronic charges close to zero. Thus, on the basis of the theoretical calculation, we find that, for all complexes, at the microscopic level in the contact region, the electronic charge is transferred from the gold atom to the contacting carbon atoms. This causes corresponding polarization of the gold atoms. In the experimental investigation of the metal−C_{60} contact region, a transfer of electronic charge from the gold surface to C_{60} was revealed.[36,44] Thus, for the C_{60}−Au complex as a whole (macroscopic level), there is a substantial amount of electronic charge transfer from the C_{60} to the gold clusters, while at the metal−surface contact region (microscopic level), electronic charge is transferred from the gold atom to the contacting carbon atoms.

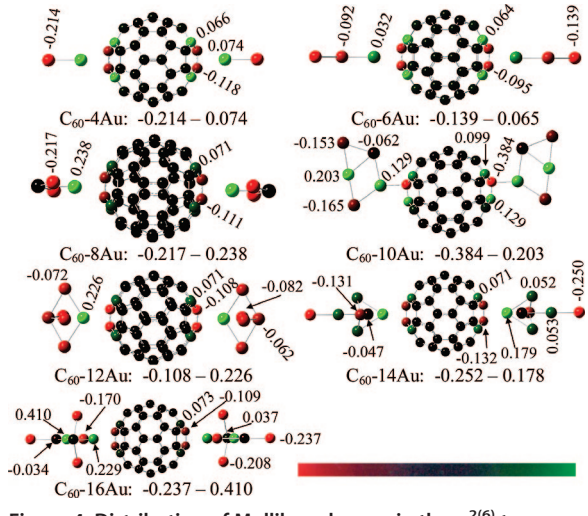

Figure 4. Distribution of Mulliken charges in the $\eta^{2(6)}$ type of C_{60}−*n*Au complexes. The red color represents the location of largest negative charge, while the green color represents the largest positive charge. The range of charge (red to green) in each plot is given next to the name of the corresponding complex. The Mulliken charges (in au) for major contributing atoms are also given.

The computed HOMO–LUMO energy gaps of the studied complexes are shown in Table 1. In our earlier calculation on C_{60} and selected carbon nanostructures at the B3LYP/6-31G(d) level of theory, it was found that the energy difference between the highest occupied molecular orbital (HOMO) and the lowest unoccupied molecular orbital (LUMO) for C_{60} is about 2.77 eV, and this energy difference was found to decreased significantly with changes in the shape and size of the carbon nanostructures.[12] The band gap of solid C_{60} is found to be 2.3 ± 0.1 eV.[45] Thus, given the agreement, the HOMO–LUMO energy difference can be approximated

as the band gap of C_{60} in the solid phase. The computed HOMO–LUMO energy gap presented in Table 1 shows that the band gaps of C_{60}−gold complexes are significantly lower than that of the isolated C_{60}. Further, for those complexes where odd numbers of gold atoms on each side of C_{60} are involved in the complex formation, the energy gap is significantly lower than for complexes involving even numbers of Au atoms. In general, with increasing size of the gold cluster, the HOMO–LUMO energy gap was found to decrease. However, it would be interesting to determine the HOMO–LUMO energy gap of complexes involving significantly bigger gold clusters, since with the larger gold clusters, the point of contact with C_{60} will also increase. This is currently under investigation in our laboratory. Satio and Oshiyama[46] have obtained the HOMO–LUMO gap of C_{60} as 1.9 eV and the band gap of face-centered-cubic C_{60} crystal as 1.5 eV. These authors performed this excellent work in 1991 using the local density approximation. At that time, geometry optimization of C_{60} at that computational level was almost impossible. The authors took the experimental parameters of fullerene, r_1 and r_2, as 1.46 and 1.40 Å, respectively) and performed single-point energy calculations. Therefore, the difference with respect to our computed result is due to the different approaches used in the investigation.

The HOMO, LUMO, and other close-lying occupied and unoccupied orbitals of C_{60}−4Au and C_{60}−6Au are shown in the Figures 5 and 6, respectively, while relevant orbitals corresponding to other complexes are provided in the Supporting Information; some selected orbitals of these complexes are shown in Figure 7. It is evident that the HOMOs of all the complexes are generally localized on metal clusters (some delocalization on C_{60} in a few complexes is also found), but the nature of the LUMOs is entirely different. In the case of those complexes where even numbers of gold atoms are present on each side of C_{60} (nAu−C_{60}−nAu; n = 2, 4, 6, and 8), the LUMO is mainly localized on C_{60}, except for the C_{60}−8Au and C_{60}−16Au complexes, where some delocalization on gold atoms is also revealed. However, for the C_{60}−6Au, C_{60}−10Au, and C_{60}−14Au complexes, the LUMO is mainly localized on gold clusters, though for C_{60}−10Au some delocalization on the carbon atoms at the contact region of C_{60} is also found. Further, analysis of the HOMOs of C_{60}−6Au, C_{60}−10Au, and C_{60}−14Au complexes shows that both sides of the Au clusters have the same orbital-phase symmetry. We also performed single-point energy as well as geometry optimization calculations for the triplet state of these complexes. Computed total energies are shown in Figures 2 and 3. It was found that, although for the C_{60}−4Au complex the ground state is singlet, for

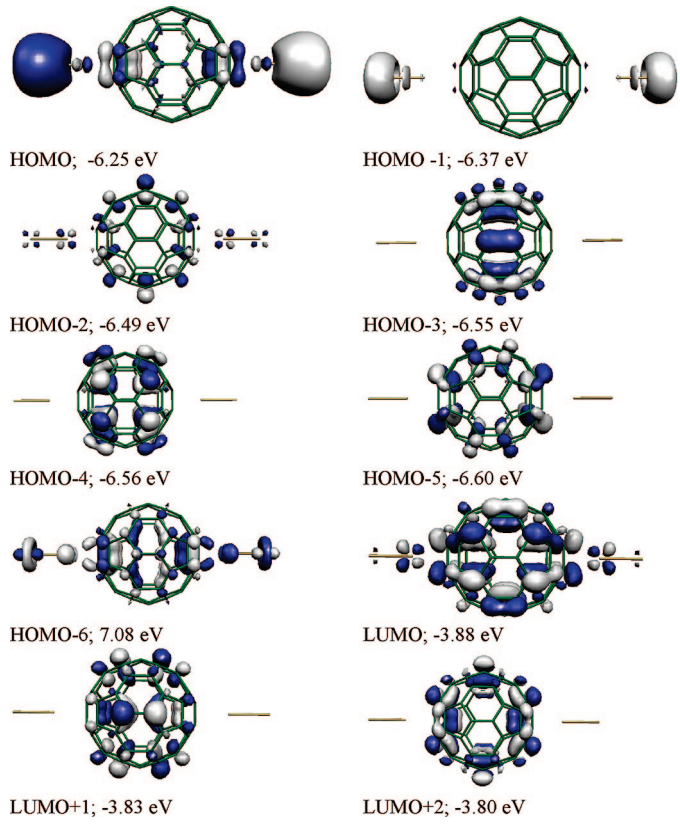

Figure 5. Frontier orbitals and orbital energies of the C_{60}−4Au complex, having $\eta^{2(6)}$-coordination.

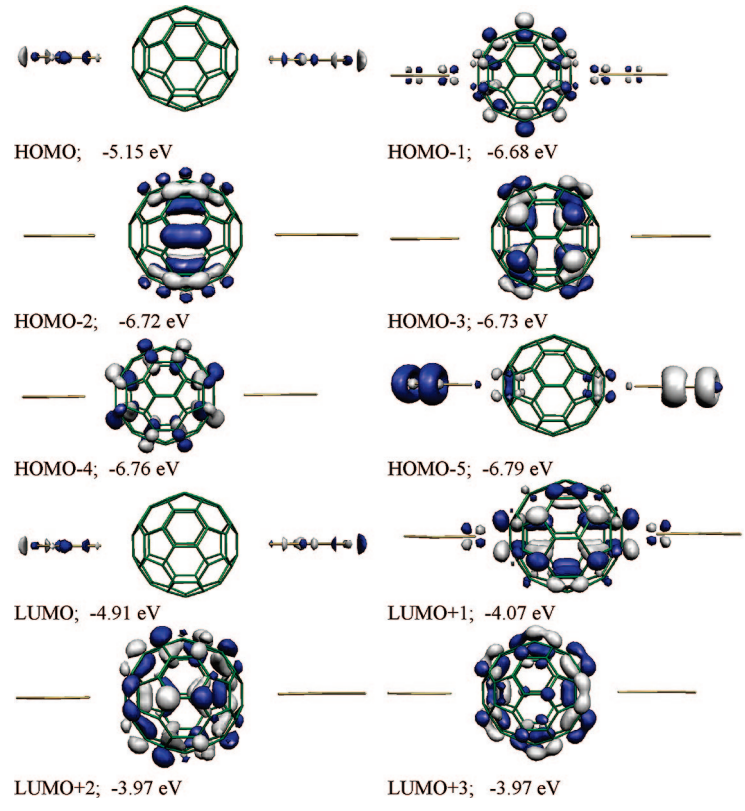

Figure 6. Frontier orbitals and orbital energies of the C_{60}−6Au complex, having $\eta^{2(6)}$-coordination.

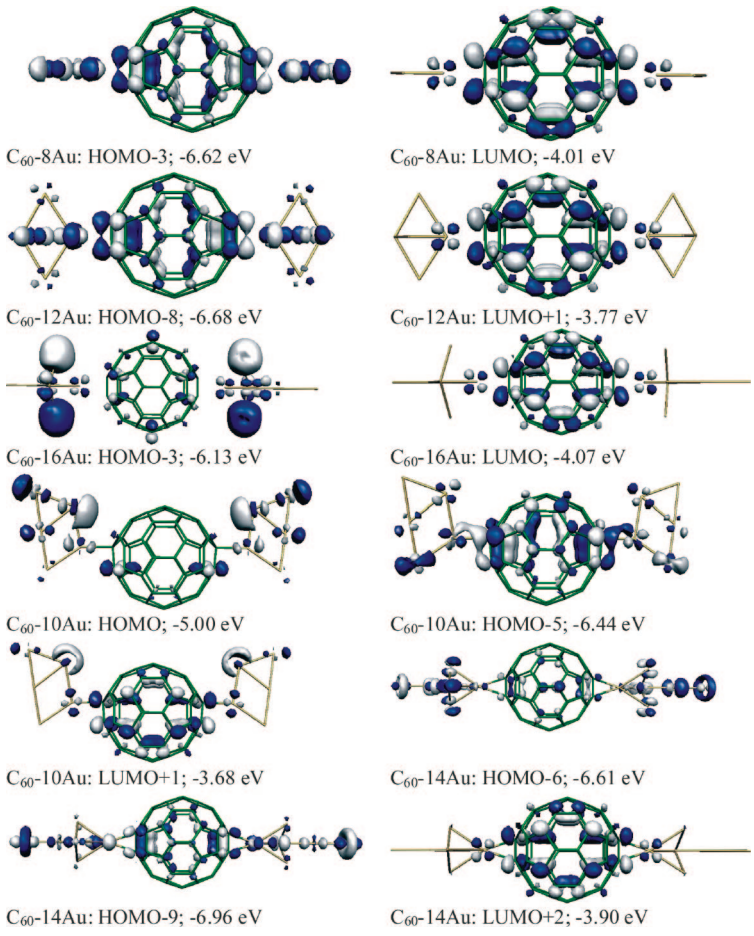

Figure 7. Some important orbitals and orbital energies of selected C_{60}−gold complexes having $\eta^{2(6)}$-coordination.

the C_{60}−6Au complex the triplet state is about 0.5 eV more stable than the corresponding singlet state. Analogous results were found for other complexes, which suggests that the singlet ground state is energetically favorable for the complexes with even numbers of gold atoms on each side of C_{60} but the triplet state is more favorable for complexes with odd numbers of gold atoms on each side of C_{60}. No significant change in the geometry of the complex under triplet ground-state optimization compared to the corresponding singlet geometry was revealed. This fact is also evident from the similarity among the energy values obtained from the single-point calculations and optimized triplet states of the respective complexes (Figures 2 and 3). In the triplet state, the band gap would correspond to the energy difference between the highest occupied and lowest unoccupied α-orbitals, and the computed band gap is shown in Table 1. Examination of the LUMO+1, LUMO+2, and LUMO+3 orbital energies of the C_{60}−6Au (Figure 6) and C_{60}−14Au (Supporting Information, Figure S5) complexes suggests that these orbitals are almost degenerate. Further, these orbitals are about 0.8 – 0.9 eV higher in energy than the corresponding LUMO orbital. It should be noted that C_{60} has three degenerate LUMO orbitals.[7] Thus, it appears that the LUMO+1, LUMO+2, and LUMO+3 orbitals generally correspond to degenerate LUMOs of C_{60}. The LUMO, LUMO+1, and LUMO+2 orbitals of each of the complexes with even numbers of gold atoms on each side of C_{60} are also nearly degenerate (maximum energy difference being about 0.1 eV); therefore, these orbitals also correspond to the degenerate LUMOs of C_{60}.

Ab initio calculations have been found to be very useful in the exploration of charge transport efficiency of molecular systems.[47–49] It has been found that those orbitals which are closely positioned near the Fermi level and delocalized throughout the entire molecule are important in facilitating the charge conduction across the molecular junction. For example, Seminario *et al.*[48] have studied the conduction properties of polyynes and alkanes and found that, due to the delocalized nature of molecular orbitals of polyynes near Fermi level, the conductance was significantly larger than that in the alkanes, although the densities of states for both systems at the Fermi energy were similar. Further, the π charge cloud associated with the C−C bond provides a route for the transport of electron currents. The same is true for C_{60}, since electron current cannot directly pass diagonally through the inside of the cage.[50]

Witek *et al.*[21] computed the energy of the Fermi level (E_{FL}) of C_{28}, C_{60}, and C_{70} by taking the average of the HOMO and LUMO orbital energies. The computed value of E_{FL} for C_{60} and C_{70} was found to be about −4.7 eV at the BLYP/cc-pVTZ and BLYP/3-21G levels and about −5.0 eV at the SCC-DFTB level, while for C_{28}, depending upon the level of the theory, it was predicted to range from −5.1 to 5.2 eV.[21] Our computed E_{FL} values for the studied complexes are shown in Table 1. The computed value for C_{60}, at −4.6 eV, is in good agreement with that obtained by Witek *et al.*[21] It is evident that gold clusters have a significant influence on the Fermi energy of C_{60} (Table 1). Since the Fermi energy of Au metal is about −5.3 eV,[39] the computed E_{FL} values of the studied complexes (in the range of −5.1 to −4.8 eV) are near the average E_{FL} of bulk Au and that of C_{60}.[21] It is evident that, for the C_{60}−4Au complex, the HOMO, HOMO−6, and LUMO orbitals are delocalized and located about 1.19 and 2.02 eV below and 1.18 eV above the Fermi level, respectively. Therefore, HOMO and LUMO orbitals of the C_{60}−4Au complex, being nearer to the Fermi level, are important for the charge transport in the system. In the case of the C_{60}−8Au complex, the HOMO−3 and LUMO orbitals, being 2.6 eV apart and about 1.7 eV below and 0.9 eV above the Fermi level, respectively, are significantly delocalized (Figure 7). Therefore, HOMO−3 and LUMO are the most important for the charge transport in the C_{60}−8Au system. For the C_{60}−12Au complex, the HOMO−8 and LU-

MO+1 will dominate for the charge transport under sufficient bias (Figure 7). Similarly, for the C_{60}−16Au complex, the HOMO−3 and LUMO orbitals will play an important role for charge transport in the system (Figure 7). Further, the HOMO−1, HOMO−5, and LUMO+1 of the C_{60}−6Au (Figure 6), the HOMO, HOMO−5, and LUMO+1 of C_{60}−10Au, and the HOMO−6 and LUMO+2 of C_{60}−14Au (Figure 7) are generally also delocalized; therefore, they are expected to contribute to the conduction of respective systems under sufficient external bias.

CONCLUSIONS

Carbon fullerene forms stable complexes with gold clusters. The complexes in which gold clusters are bonded at the top of the center of fused six-membered rings ($\eta^{2(6)}$-type coordination) are significantly more stable than those bonded at the top of the center of fused six- and five-membered rings ($\eta^{2(5)}$-type coordination). A significant amount of charge transfer from C_{60} to gold clusters was revealed, suggesting an electrostatic type of interaction between the components of the clusters. However, at the microscopic level near the nanojunction, electronic charge is transferred from the gold atom to the interacting carbon atoms of C_{60}. The ground state of complexes involving odd numbers of gold atoms on each side of C_{60} was found to be triplet, while for those complexes involving even numbers of gold atoms, the ground state was revealed to be characterized by singlet configuration. The HOMO–LUMO energy gap was predicted to decrease with increase in the size of the cluster. Some orbitals near the Fermi level were found to be delocalized and thus will contribute to the electronic conduction of the system.

COMPUTATIONAL DETAILS

Molecular geometries of complexes were optimized at the DFT level using Becke's[51] three-parameter nonlocal hybrid exchange potential with the nonlocal correlation functional of Lee, Yang, and Parr (B3LYP).[52] The standard 6-31G(d) basis set was used for carbon atoms, while the LANL2DZ effective core potential (ECP) was used for gold atoms. Geometries of complexes were generally optimized under the C_{2h} symmetry. It is well-known that the computation of interaction energy with finite basis sets introduces error known as basis set superposition error (BSSE). Since interaction energy is defined as the energy difference between the complex and the constituent monomers, the BSSE error arises due to the fact that different numbers of basis functions are used to describe the complex and monomers for the same basis set. Due to the larger number of basis functions, the complex has comparatively lower energy that the sum of its components. The BSSE-corrected interaction energy was computed using the Boys–Bernardi counterpoise correction scheme.[53] The interaction energies of complexes were computed from the three-body terms given by eq 1:

$$E_{int} = E_{ABC} - E_{A(ABC)} - E_{B(ABC)} - E_{C(ABC)} \quad (1)$$

where E_{int} represents the interaction energy, E_{ABC} is the total energy of the complex, $E_{B(ABC)}$ represents the total energy of the C_{60} with ghost atoms in place of the rest of the system, and $E_{A(ABC)}$ and $E_{C(ABC)}$ represent the total energy on either side of the gold clusters of the complex with ghost atoms for the rest of the system. The BSSE correction is important to determine the stability of complexes correctly. All calculations were performed using the Gaussian 03 suite of programs,[54] while molecular orbitals were visualized using the Molekel program.[55]

Acknowledgment. M.K.S. and J.L. are thankful to financial support from Army Research Laboratory BAA no. DAAD19-03-R-0017, section 2.41, Contract No. W911QX-07-C-0100, NSF-CREST grant no. HRD-0318519, ONR grant no. N00034-03-1-0116, and the Mississippi Center for Supercomputing Research (MCSR) for the generous computational facility.

Supporting Information Available: Figures S1−S6, showing frontier orbitals and orbital energies of C_{60} and C_{60}−gold complexes; complete ref 54. This material is available free of charge *via* the Internet at http://pubs.acs.org.

REFERENCES AND NOTES

1. Kroto, H. W.; Heath, J. R.; O'Brien, S. C.; Curl, R. F.; Smalley, R. E. C_{60}: Buckminsterfullerene. *Nature* **1985**, *318*, 162–163.
2. Endo, M. Tailoring Carbon Nano Structures: Nanocarbons and Nanodevices. *Mol. Cryst. Liq. Cryst.* **2002**, *386*, 159–166.
3. Bosi, S.; Ros, T. D.; Spalluto, G.; Prato, M. Fullerene Derivatives: An Attractive Tool for Biological Applications. *Eur. J. Med. Chem.* **2003**, *38*, 913–923.
4. Palacios, J. J.; Perez-Jimenez, A. J.; Louis, E.; SanFabian, E.; Verges, J. A.; Garcia, J. A. Molecular Electronics with Gaussian98/03. In *Computational Chemistry, Reviews of Current Trends*; Leszczynski, J., Ed.; World Scientific: Singapore, 2005; Vol. 9, pp 1–46.
5. Di Ventra, M. Molecules as Components in Electronic Devices: A First-Principles Study. In *Computational Chemistry, Reviews of Current Trends*; Leszczynski, J., Ed.; World Scientific: Singapore, 2002; Vol. 7, pp 1–15.
6. Halford, B. Fullerene for the Face. *Chem. Eng. News* **2006**, *84* (13), 47.
7. Balch, A. L.; Olmstead, M. M. Reactions of Transition Metal Complexes with Fullerenes (C_{60}, C_{70}, etc.) and Related Materials. *Chem. Rev.* **1998**, *98*, 2123–2166.
8. Ajayan, P. M. Nanotubes from Carbon. *Chem. Rev.* **1999**, *99*, 1787–1800.
9. Daniel, M.-C.; Astruc, D. Gold Nanoparticles: Assembly, Supramolecular Chemistry, Quantum-Size-Related Properties, and Applications toward Biology, Catalysis, and Nanotechnology. *Chem. Rev.* **2004**, *104*, 293–346.
10. Teo, B. K.; Sun, X. H. Silicon-Based Low-Dimensional Nanomaterials and Nanodevices. *Chem. Rev.* **2007**, *107*, 1454–1532.
11. Brust, M.; Kiely, C. J. Some Recent Advances in Nanostructure Preparation from Gold and Silver: A Short Topical Review. *Colloids Surf. A: Physicochem. Eng. Asp.* **2002**, *202*, 175–186.
12. Shukla, M. K.; Leszczynski, J. A Density Functional Theory Study on the Effect of Shape and Size on the Ionization Potential and Electron Affinity of Different Carbon Nanostructures. *Chem. Phys. Lett.* **2006**, *428*, 317–320.
13. Banin, U.; Cao, Y. W.; Katz, D.; Millo, O. Identification of Atomic-Like Electronic States in Indium Arsenide Nanocrystal Quantum Dots. *Nature* **1999**, *400*, 542–544.
14. Bockrath, M.; Cobden, D. H.; Lu, J.; Rinzler, A. G.; Smalley, R. E.; Balents, L.; McEuen, P. L. Luttinger-Liquid Behaviour in Carbon Nanotubes. *Nature* **1999**, *397*, 598–601.
15. Stipe, B. C.; Rezaei, M. A.; Ho, W. Single-Molecule Vibrational Spectroscopy and Microscopy. *Science* **1998**, *280*, 1732–1735.
16. Park, H.; Park, J.; Lim, A. K. L.; Anderson, E. H.; Alivisatos, A. P.; McEuen, P. L. Nanomechanical Oscillations in a Single-C_{60} Transistor. *Nature* **2000**, *407*, 57–60.

17. Jorn, R.; Seideman, T. Theory of Current-Induced Dynamics in Molecular-Scale Devices. *J. Chem. Phys.* **2006**, *124*, 84703-1–84703-11.
18. Kaun, C. -C.; Seideman, T. Current-Driven Oscillations and Time-Dependent Transport in Nanojunctions. *Phys. Rev. Lett.* **2005**, *94*, 226801-1–226801-4.
19. Alavi, S.; Larade, B.; Taylor, J.; Guo, H.; Seideman, T. Current-Triggered Vibrational Excitation in Single-Molecule Transistors. *Chem. Phys.* **2002**, *281*, 293–303.
20. Yan, L.; Seminario, J. M. Electron Transport in Nano-Gold-Silicon Interfaces. *Int. J. Quantum Chem.* **2007**, *107*, 440–450.
21. Witek, H. A.; Irle, S.; Zheng, G.; de Jong, W. A.; Morokuma, K. Modeling Carbon Nanostructures with the Self-Consistent Charge Density-Functional Tight-Binding Method: Vibrational Spectra and Electronic Structure of C_{28}, C_{60} and C_{70}. *J. Chem. Phys.* **2006**, *125*, 214706-1–214706-26.
22. Peralta-Inga, Z.; Boyd, S.; Murray, J. S.; O'Connor, C. J.; Politzer, P. Density Functional Tight-Binding Studies of Carbon Nanotube Structures. *Struct. Chem.* **2003**, *14*, 431–443.
23. Palacios, J. J. Coulomb Blockade in Electron Transport Through a C_{60} Molecule from First Principles. *Phys. Rev. B* **2005**, *72*, 125424-1–125424-6.
24. Palacios, J. J.; Perez-Jimenez, A. J.; Louis, E.; SanFabian, E.; Verges, J. A. First-Principles Phase-Coherent Transport in Metallic Nanotubes with Realistic Contacts. *Phys. Rev. Lett.* **2003**, *90*, 106801-1–106801-4.
25. Palacios, J. J.; Louis, E.; Perez-Jimenez, A. J.; SanFabian, E.; Verges, J. A. An Ab Initio Approach to Electrical Transport in Molecular Devices. *Nanotechnology* **2002**, *13*, 378–381.
26. Palacios, J. J.; Perez-Jimenez, A. J.; Louis, E.; Verges, J. A. Electronic Transport Through C_{60} Molecules. *Nanotechnology* **2001**, *12*, 160–163.
27. Nakamura, H.; Yamashita, K. An Efficient Molecular Orbital Approach for Self-Consistent Calculations of Molecular Junctions. *J. Chem. Phys.* **2006**, *125*, 194106-1–194106-12.
28. Sergueev, N.; Roubtsov, D.; Guo, H. *Ab Initio* Analysis of Electron-Phonon Coupling in Molecular Devices. *Phys. Rev. Lett.* **2005**, *95*, 146803-1–146803-4.
29. Frank, S.; Poncharal, P.; Wang, Z. L.; de Heer, W. A. Carbon Nanotube Quantum Resistors. *Science* **1998**, *280*, 1744–1746.
30. Bachtold, A.; Fuhrer, M. S.; Plyasunov, S.; Forero, M.; Anderson, E. H.; Zettl, A.; McEuen, P. L. Scanned Probe Microscopy of Electronic Transport in Carbon Nanotubes. *Phys. Rev. Lett.* **2000**, *84*, 6082–6085.
31. Nygard, J.; Cobden, D. H.; Lindelof, P. E. Kondo Physics in Carbon Nanotubes. *Nature* **2000**, *408*, 342–346.
32. Berdinsky, A. S.; Fink, D.; Yoo, J. B.; Chadderton, L. T.; Chun, H. G.; Han, J. H.; Dragunov, V. P. Electronic Conduction Properties of Au/C_{60}/p-Si and C_{60}/Au/p-Si Sandwich Structures: I–V and Transducer Characteristics. *Solid State Commun.* **2004**, *130*, 809–814.
33. Koltun, M.; Faiman, D.; Goren, S.; Katz, E. A.; Kunoff, E.; Shames, A.; Shtutina, S.; Uzan, B. Solar Cells from Carbon. *Sol. Energy Mater. Sol. Cells* **1996**, *44*, 485–491.
34. Kong, B.-S.; Jung, D.-H.; Oh, S.-K.; Han, C.-S.; Jung, H.-T. Single-Walled Carbon Nanotube Gold Nanohybrids: Application in Highly Effective Transparent and Conductive Films. *J. Phys. Chem. C* **2007**, *111*, 8377–8382.
35. Andriotis, A. N.; Menon, M. Geometry and Bonding in Small $(C_{60})_nNi_m$ Clusters. *Phys. Rev. B* **1999**, *60*, 4521–4524.
36. Lyon, J. T.; Andrews, L. Infrared Spectrum of the Au-C_{60} Complex. *ChemPhysChem* **2005**, *6*, 229–232.
37. Lichtenberger, D. L.; Wright, L. L.; Gruhn, N. E.; Rempe, M. E. Electronic Structure and Bonding of C_{60} to Metals. *Synth. Met.* **1993**, *59*, 353–367.
38. Lichtenberger, D. L.; Wright, L. L.; Gruhn, N. E.; Rempe, M. E. Electronic Structure of Exohedral Interactions Between C_{60} and Transition Metals. *J. Organomet. Chem.* **1994**, *478*, 213–221.
39. Seminario, J. M.; De La Cruz, C. E.; Derosa, P. A. A Theoretical Analysis of Metal−Molecule Contacts. *J. Am. Chem. Soc.* **2001**, *123*, 5616–5617.
40. Altman, E. I.; Colton, R. J. Nucleation, Growth, and Structure of Fullerene Films on Au(111). *Surf. Sci.* **1992**, *279*, 49–67.
41. Altman, E. I.; Colton, R. J. Determination of the Orientation of C_{60} Adsorbed on Au(111) and Ag(111). *Phys. Rev. B* **1993**, *48*, 18244–18249.
42. Tzeng, C.-T.; Lo, W.-S.; Yuh, J.-Y.; Chu, R.-Y.; Tsuei, K.-D. Photoemission, Near-Edge X-Ray-Absorption Spectroscopy, and Low-Energy Electron-Diffraction Study of C_{60} on Au(111) surfaces. *Phys. Rev. B* **2000**, *61*, 2263–2272.
43. Kumar, A.; Mishra, P. C.; Suhai, S. Binding of Gold Clusters with DNA Base Pairs: A Density Functional Theory of Neutral and Anionic GC-Au_n and AT-Au_n (n = 4,8) Complexes. *J. Phys. Chem. A* **2006**, *110*, 7719–7727.
44. Baxter, R. J.; Rudolf, P.; Teobaldi, G.; Zerbetto, F. Modelling of the Adsorption of C_{60} on the Au(110) Surface. *ChemPhysChem* **2004**, *5*, 245–248.
45. Lof, R. W.; van Veenendaal, M. A.; Koopmans, B.; Jonkman, H. T.; Sawatzky, G. A. Band Gap, Excitons, and Coulomb Interaction in Solid C_{60}. *Phys. Rev. Lett.* **1992**, *68*, 3924–3927.
46. Satio, S.; Oshiyama, A. Cohesive Mechanism and Energy Bands of Solid C_{60}. *Phys. Rev. Lett.* **1991**, *66*, 2637–2640.
47. Derosa, P. A.; Seminario, J. M. Electron Transport through Single Molecules: Scattering Treatment Using Density Functional and Green Functional Theories. *J. Phys. Chem. B* **2001**, *105*, 471–481.
48. Seminario, J. M.; De La Cruz, C.; Derosa, P. A.; Yan, L. Nanometer-Size Conducting and Insulating Molecular Devices. *J. Phys. Chem. B* **2004**, *108*, 17879–17885.
49. Seferos, D. S.; Trammell, S. A.; Bazan, G. C.; Kushmerick, J. G. Probing π-Coupling in Molecular Junctions. *Proc. Natl. Acad. Sci. U.S.A.* **2005**, *102*, 8821–8825.
50. Ono, T.; Hirose, K. First-Principles Study of Electron-Conduction Properties of C_{60} Bridges. *Phys. Rev. Lett.* **2007**, *98*, 26804-1–26804-4.
51. Becke, A. D. Density-Functional Thermochemistry. III. The Role of Exact Exchange. *J. Chem. Phys.* **1993**, *98*, 5648–5652.
52. Lee, C.; Yang, W.; Parr, R. G. Development of the Colle−Salvetti Correlation-Energy Formula into a Functional of the Electron Density. *Phys. Rev. B* **1988**, *37*, 785–789.
53. Boys, S. F.; Bernardi, F. The Calculation of Small Molecular Interactions by the Differences of Separate Total Energies. Some Procedures with Reduced Errors. *Mol. Phys.* **1970**, *19*, 553–566.
54. Frisch, M. J.; Trucks, G. W.; Schlegel, H. B.; Scuseria, G. E.; Robb, M. A.; Cheeseman, J. R.; Montgomery, J. A., Jr.; Vreven, T.; Kudin, K. N.; Burant, J. C.; *et al. Gaussian 03*, Revision D.01; Gaussian, Inc.: Wallingford, CT, 2004.
55. Flükiger, P.; Lüthi, H. P.; Portmann, S.; Weber, J. *MOLEKEL 4.3.*; Swiss Center for Scientific Computing: Manno, Switzerland, 2000 (www.cscs.ch/molekel).